

# A dynamical transition from localized to uniform scrambling in locally hyperbolic systems

Mathias Steinhuber,<sup>1</sup> Peter Schlagheck,<sup>2</sup> Juan Diego Urbina,<sup>1</sup> and Klaus Richter<sup>1</sup>

<sup>1</sup>*Institut für Theoretische Physik, Universität Regensburg, 93040 Regensburg, Germany*

<sup>2</sup>*CESAM Research Unit, University of Liege, 4000 Liège, Belgium*

(Dated: March 28, 2023)

Fast scrambling of quantum correlations, reflected by the exponential growth of Out-of-Time-Order Correlators (OTOCs) on short pre-Ehrenfest time scales, is commonly considered as a major signature of quantum chaos in quantum systems with a classical limit. In two recent works, by Hummel et al. [1] and by Scaffidi et al. [2], a significant difference in the scrambling rate of integrable (many-body) systems was observed, depending on the initial state being semiclassically localized around unstable fixed points or fully delocalized (infinite temperature). Specifically, the quantum Lyapunov exponent  $\lambda_q$  quantifying the OTOC growth is given, respectively, by  $\lambda_q = 2\lambda_s$  or  $\lambda_q = \lambda_s$  in terms of the stability exponent  $\lambda_s$  of the hyperbolic fixed point. Here we show that a wave packet, initially localized around this fixed point, features a distinct *dynamical* transition between these two regions. We present an analytical semiclassical approach providing a physical picture of this phenomenon and support our findings by extensive numerical simulations in the whole parameter range of locally unstable dynamics of a Bose-Hubbard dimer. Our results suggest that the existence of this transition is a hallmark of unstable separatrix dynamics in integrable systems. This allows one to distinguish, within the exponential OTOC growth behavior, unstable integrable (many-body) dynamics from genuine chaotic dynamics featuring uniform growth.

## I. INTRODUCTION

The scrambling of quantum correlations is an ubiquitous phenomenon across the physics of interacting many-body systems [3, 4]. Its connection to quantum chaos has been established in systems ranging from models for black holes [5–8] to realistic many-body systems such as the SYK-model [9], even comprising systems without a classical limit [10]. Due to the appealing connection with the powerful concepts of quantum chaos, Out-of-Time-Ordered Correlators (OTOCs) [11] represent a major probe of scrambling and thus have received a swiftly increasing huge theoretical interest [3, 5] that has driven efforts for experimental proposals [12] and realizations [13, 14].

In systems with a semiclassical regime, fast scrambling is considered an unambiguous indicator of classical (mean-field) instabilities [4]. As such, Bose-Hubbard systems, with their well understood and controlled classical (mean-field) limit and a large semiclassical region of state space, are prime models to study imprints of scrambling [15–17]. Recently it was shown [1, 18] that an initial exponential growth of OTOCs does not necessarily imply chaotic dynamics of the system’s classical counterpart, *i.e.* such OTOC behavior alone cannot serve as clear-cut probe of quantum chaos. These works [1, 18] and further ones picking up the same idea [2, 19, 20] show that for quantum (many-body) systems with a classical limit and a semiclassical regime it is sufficient to have local instabilities in a (possibly integrable) phase space to generate exponentially growing OTOCs. Several examples of this situation have been numerically studied [21, 22], including basic models such as an inverted harmonic oscillator [23].

Generically, the prime example of the mechanism for an exponential OTOC growth in an integrable system in

the existence of an unstable (hyperbolic) fixed point. Although, by definition, all Lyapunov exponents  $\lambda_L$  are zero in integrable systems, the classical dynamics around fixed points is locally hyperbolic if they have at least one positive stability exponent  $\lambda_s > 0$ . This type of instability will be considered here. In the early time regime, defined up to a time scale depending logarithmically on the effective Planck constant  $\hbar_{\text{eff}}$ , the OTOCs involving dynamics around unstable points of many-body integrable systems display two markedly different behaviors. In Refs. [1] and [2], the quantum Lyapunov exponents  $\lambda_q$  quantifying the OTOC growth rate are compared to the stability exponents of dominant unstable fixed points of the corresponding classical mean-field dynamics yielding good agreement with  $2\lambda_s$  [1] or  $\lambda_s$  [2], respectively.

In this paper we resolve this apparent discrepancy with regard to the operator growth and provide a unified dynamical mechanism explaining the two results in a comprehensive way. We demonstrate that there is a universal  $2\lambda_s$  to  $\lambda_s$  transition for the OTOC growth rate  $\lambda_q$  for dynamics around unstable fixed points in the pre-Ehrenfest time regime which interpolates between these two limits. Furthermore, the crossover develops a kink in the strictly classical limit  $\hbar_{\text{eff}} \rightarrow 0$ . Moreover, we show that this  $2\lambda_s$  to  $\lambda_s$  transition is related to an underlying dynamical transition of the initial quantum state in a phase-space representation and argue that the  $2\lambda_s$  to  $\lambda_s$  transition is a hallmark of integrable systems. We propose that this effect can thus be used to distinguish chaotic and integrable systems by properly analyzing the growth behavior of OTOCs at pre-Ehrenfest time scales.

The paper is structured into three further sections. In Sec. II, we present a heuristic argument for OTOCs to exhibit different exponential regimes and the corresponding  $2\lambda_s$  to  $\lambda_s$  transition. In order to verify the picture

put forward, we perform an extensive study of the Bose-Hubbard dimer in Sec. III. There, we start with the definition of the dimer and a study of the classical mean-field system including an analytical study of the classical OTOC. Then, numerical results for the OTOCs follow obtained from extensive simulations that display excellent agreement with the classical results for the OTOCs. Furthermore, we show how one can tune the  $2\lambda_s$  to  $\lambda_s$  transition, and study its robustness with regard to changing the system parameters. In Sec. IV we summarize our findings and discuss their possible extension to non-integrable systems.

## II. OUT-OF-TIME-ORDER CORRELATOR IN INTEGRABLE SYSTEMS WITH LOCAL HYPERBOLICITY

Our goal in this section is to refine the pre-Ehrenfest theory for scrambling around hyperbolic fixed points in integrable systems. In particular we attempt to relax the localization properties of the initial state considered in [1, 2]. The OTOC for two operators  $\hat{A}, \hat{B}$  with respect to a state  $\hat{\rho}$  is defined by

$$\mathbf{C}(t) = \text{tr} \{ \hat{\rho} |[\hat{A}(t), \hat{B}]|^2 \}, \quad (1)$$

which is by itself a modulus-squared commutator. When this squared commutator is expanded in individual correlators one obtains, besides contributions that admit a standard time ordering, extra irreducibly un-ordered correlations [5], with anomalous dynamical behavior that are the central object of study.

The long-time (post-Ehrenfest) saturation of generic OTOCs has been subject of several studies, both in the chaotic [24, 25] and integrable [1, 26] regimes where interference effects beyond a pure quasiclassical (Truncated-Wigner like-) approach appear [27].

Here, however, our focus is the short time scales, where a quasiclassical approach based on the Wigner-Moyal expansion, which is a regular expansion around  $\hbar_{\text{eff}} = 0$  [28–30], is perfectly appropriate. Keeping only leading-order terms in  $\hbar_{\text{eff}}$ , one obtains

$$\begin{aligned} \mathbf{C}(t) = \hbar_{\text{eff}}^2 \langle W_{\rho}(\vec{q}_0, \vec{p}_0) | \{ A_W(\vec{q}_0, \vec{p}_0, t), B_W(\vec{q}_0, \vec{p}_0) \} |^2 \rangle_{\text{PS}} \\ + O(\hbar_{\text{eff}}^4), \end{aligned} \quad (2)$$

where  $A_W, B_W$  are the Wigner-transforms of the operators  $\hat{A}, \hat{B}$  and  $W_{\rho}(\vec{q}_0, \vec{p}_0)$  is the Wigner-distribution corresponding to the state  $\hat{\rho}$ .

Further,  $\langle \cdot \rangle_{\text{PS}}$  indicates integration over the whole classical (mean-field) phase space parametrized by the canonical pairs  $(\vec{q}_0, \vec{p}_0)$ . The Heisenberg time dynamics of the quantum operator is mapped to time dynamics of the classical observable  $A(q_0, p_0, t) = A(q(q_0, p_0, t), p(q_0, p_0, t))$  which arises from the classical propagation of the initial values  $q_0$  and  $p_0$ .

The effective Plank constant  $\hbar_{\text{eff}}$  has different expressions in different contexts. It is given by the usual Plank constant divided a typical action  $\hbar/S_{\text{typ}}$  in single particle cases [31–33], and the inverse of the total spin quantum number  $1/S$  for spin systems [34, 35]. In the case of interest here, interacting bosonic systems,  $\hbar_{\text{eff}} = \frac{1}{N}$  is given by the inverse of the total particle number  $N$  after convenient rescaling of the interaction strength [4, 36].

Without loss of generality, we choose the operators  $\hat{A} = \hat{q}$  and  $\hat{B} = \hat{p}$ , as they are hermitian and their classical counterparts are generalized coordinates or momenta. Therefore, at leading order in the Wigner-Moyal expansion, Eq. (2), we drop the index  $W$  and take the pure classical phase space functions. This choice of the operators simplifies the classical Poisson-brackets, that are now given by an element of the stability matrix  $\frac{\partial \vec{x}(t)}{\partial \vec{x}(0)}$  with  $\vec{x} = (\vec{q}, \vec{p})$  [37, 38].

The classical limit of the OTOC in Eq. (2) is so far a completely general result. Under the assumption of local instability, however, the leading order of exponential growth is given by the maximal local exponent  $\lambda(\vec{q}_0, \vec{p}_0)$  of the stability matrix:

$$\mathbf{C}(t) \sim \hbar_{\text{eff}}^2 \langle W_{\rho}(\vec{q}_0, \vec{p}_0) \exp \{2\lambda(\vec{q}_0, \vec{p}_0)t\} \rangle_{\text{PS}}. \quad (3)$$

At this point, it is convenient to introduce two local time-scales:

- After the local ergodic time  $\tau_s = 1/\lambda(\vec{q}_0, \vec{p}_0)$ , the exponential growth of the OTOC begins to be visible. Before  $\tau_s$ , we have sub-exponential/polynomial behavior linked to system-specific mechanisms.
- The Wigner-Weyl approximation breaks down when the leading order of the integrand in Eq. (2) becomes large compared to  $\hbar_{\text{eff}}^2$ . This breakdown defines the local Ehrenfest time  $\tau_E = \lambda^{-1}(\vec{q}_0, \vec{p}_0) \log(1/\hbar_{\text{eff}})$  and in our many-body case  $\tau_E = \lambda^{-1}(\vec{q}_0, \vec{p}_0) \log N$ .

We exploit the experimentally tunable localization features of quantum mechanical states [39] as a tool to probe the local unstable dynamics around a hyperbolic fixed point (FP) and consider a coherent-like state  $\hat{\rho}$  centered around it. In the linearized region around the FP the dynamics can be precisely described, and we can express  $\lambda(\vec{q}_0, \vec{p}_0)$  by the maximal stability exponent  $\lambda_s$  of the FP. In general, however, the linearized region is bounded and we express this by the fact that the relation  $\{A(\vec{q}_0, \vec{p}_0, t), B(\vec{q}_0, \vec{p}_0)\} = e^{\lambda_s t}$  is valid only if the unstable manifold coordinate/projection  $u(\vec{q}_0, \vec{p}_0)$  is smaller than a threshold  $c > 0$ . For times larger than zero, the exponential growth  $u(\vec{q}_0, \vec{p}_0, t) = u(\vec{q}_0, \vec{p}_0)e^{\lambda_s t}$  is only valid if the linearized region  $u(\vec{q}(t), \vec{p}(t), t) < c$  is still fulfilled. Afterwards we need to replace the time dynamics of the unstable manifold by a sub-exponential function. We refer to this mechanism as a kind of *leaking* from the linearized region [2].

The key observation is that, although the sub-exponential function describes the classical evolution outside and it is therefore negligibly small compared to the

exponential growth in the linearized region, its contribution is weighted by a portion of phase space that grows exponentially. These considerations allow us to heuristically account for the leaking mechanism, by modifying the Eq. (3) as

$$C(t) \sim \hbar_{\text{eff}}^2 e^{2\lambda_s t} \langle W_\rho(\vec{q}_0, \vec{p}_0) \Theta(c - e^{\lambda_s t} u(\vec{q}_0, \vec{p}_0)) \rangle_{\text{LR}}, \quad (4)$$

where we restrict the phase-space integration to the dominant linearized region (LR) around the FP.

For definiteness, let us consider now a Gaussian wave-packet with an initial linear width  $\Delta u$  along the unstable manifold  $u(\vec{q}, \vec{p})$ . In this situation, the wave-packet reaches the boundary of the linear region by a finite time  $\tau_L = \lambda_s^{-1} \log(c/\Delta u)$ , which we correspondingly call the leaking time. After  $\tau_L$ , we must take the leaking of the wave-packet into account, i.e., the phase-space volume causing the exponential growth shrinks exponentially with  $e^{-\lambda_s t}$ , i.e.,

$$\langle W_\rho(\vec{q}_0, \vec{p}_0) \Theta(c - e^{\lambda_s t} u(\vec{q}_0, \vec{p}_0)) \rangle_{\text{LR}} \sim \begin{cases} \text{const.}, & t < \tau_L \\ e^{-\lambda_s t}, & t > \tau_L \end{cases}.$$

Hence, the exponential growth of the OTOC in Eq. (4) decreases to  $e^{\lambda_s t}$ . This finally leads to a short-time behavior of the OTOC around an unstable fixed point given by

$$C(t) \sim \begin{cases} \text{poly.}, & t < \tau_s \\ e^{2\lambda_s t}, & \tau_s < t < \tau_L \\ e^{\lambda_s t}, & \tau_L < t < \tau_E \\ \text{osc.}, & \tau_E < t \end{cases}, \quad (5)$$

that is schematically displayed in Fig. 1 showing two exponential regions.

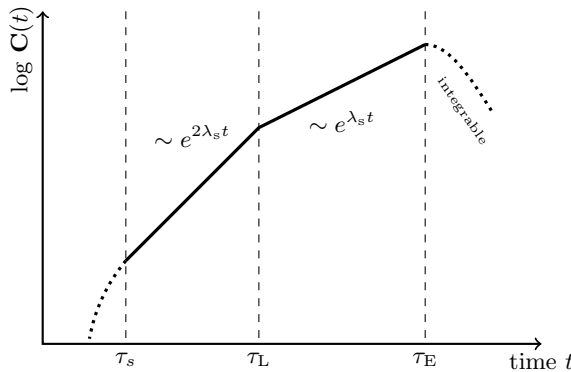


FIG. 1. Expected behavior of an OTOC centered at a FP if  $\tau_s < \tau_L < \tau_E$ : OTOCs grow polynomial for times shorter  $\tau_s$ , exponential with  $2\lambda_s$  for times shorter  $\tau_L$ , exponential with  $\lambda_s$  for times shorter  $\tau_E$ , but greater than  $\tau_L$ . Post-Ehrenfest time scales display oscillatory behaviour if the system is integrable [26] and saturation if the system is chaotic [24, 40].

It is important to note that there is a hierarchy of time scales: the leaking time is only relevant if  $\tau_L <$

$\tau_E$ , otherwise the Wigner-Weyl approximation (in leading order), see Eq. (2), is already invalid.

The initial linear width  $\Delta u$  scales with some power  $\hbar_{\text{eff}}^\alpha$  for typical states. This gives an asymptotic expression for the leaking time by  $\tau_L \sim \frac{\alpha}{\lambda_s} \log N + O(\log(c))$ . Hence, we have a direct proportional relation to the Ehrenfest time  $\tau_L \sim \alpha \tau_E$  for  $\hbar_{\text{eff}} \rightarrow 0$ .

We see then, that one can clearly distinguish three parametric regions:  $\tau_L < \tau_s$ ,  $\tau_s < \tau_L < \tau_E$  and  $\tau_E \leq \tau_L$  (which is equivalent to  $\alpha \approx 0, < 1, \approx 1$ ):

ii) Delocalized/uniform states:  $\tau_L < \tau_s$ ,  $\alpha \approx 0$

We need to assume the FP we chose is the only unstable FP of the classical dynamics. Then, the OTOC is still governed by Eq. (5) and the  $e^{2\lambda_s t}$ -regime vanishes. A typical examples here are high temperature states ( $T \rightarrow \infty$ ).

ii) Localized states:  $\tau_s < \tau_L < \tau_E$ ,  $0 < \alpha < 1$

In this case we have the  $2\lambda_s - \lambda_s$  transition and asymptotically (for  $N \rightarrow \infty$ ) we expect a sharp kink to appear at  $\tau_L$ . The prime example are the coherent states centered at a FP. They usually have a linear size of  $\hbar_{\text{eff}}^{1/2}$  in all phase space directions.

iii) Well-localized states:  $\tau_L \approx \tau_E$ ,  $\alpha \approx 1$

The second  $e^{2\lambda_s t}$ -region is vanishing, only the one  $e^{2\lambda_s t}$ -region is visible. Fock states are candidates for the third class. Their linear width is  $\hbar_{\text{eff}}$  in the classical occupation numbers, such that  $\alpha \approx 1$  if the unstable manifold is aligned in the parallel direction.

The case  $\alpha > 1$  is unphysical and can be excluded. The uncertainty principle requires the product of the width in all directions to be  $\geq \frac{\hbar_{\text{eff}}}{2}$ . Hence if  $\alpha > 1$ , one direction must increase if  $\hbar_{\text{eff}} \rightarrow 0$ , i.e., this direction becomes delocalized if we approach the classical limit contradicting that the state is associated by a well-defined point in phase space.

At this point, we can explain the dynamical behavior of OTOCs reported in [1] and [2]. In the first paper, the authors investigated a number-projected coherent state which is simultaneously a Fock state. Its unstable manifold is parallel to the occupation direction [41], therefore it falls into the case iii) and they see only the  $2\lambda_s$ -exponential window. Correspondingly, the authors of the second paper use the infinite temperature state, hence their state directly falls into the first case and the only exponential window is given by  $e^{\lambda_s t}$ .

In the next section, we numerically explore the validity Eq. (5) for a Bose-Hubbard dimer, with the aim of carefully investigate the new case ii), where the hierarchy of time scales  $\tau_s < \tau_L < \tau_E$  implies, from our analysis, the presence of a  $2\lambda_s - \lambda_s$  transition.

### III. BOSE-HUBBARD DIMER

The Bose-Hubbard dimer describes bosonic degrees of freedom occupying on two discrete levels or sites. Prime physical setups are individual Josephson-junctions [42] or cold atoms within a small two-sited optical lattice [43–48]. In all these cases, one ends with an effective description in terms of the following Hamiltonian

$$\hat{H} = -2J(\hat{a}_2^\dagger \hat{a}_1 + \hat{a}_2 \hat{a}_1^\dagger) + \frac{g}{2}(\hat{a}_1^\dagger \hat{a}_1^2 + \hat{a}_2^\dagger \hat{a}_2^2), \quad (6)$$

where the parameter  $J$  is the hopping and  $g$  is the (local) interaction strength between particles given in units of energy. Our Hamiltonian differs from the usual dimer Hamiltonian, the hopping coefficient  $2J$  (instead of  $J$ ) is motivated to be consistent with a ring topology for higher number of wells. Consequently, the two-site ring has a doubled counted hopping term. We also introduce a new dimensionless parameter  $\Theta$  with  $J = \epsilon_0 \cos \Theta$  and  $g = \epsilon_0 \frac{2}{N} \sin \Theta$ . Using  $\Theta$  fixes the scale of the parameters to  $\epsilon_0 = \sqrt{J^2 + (\frac{gN}{2})^2}$  in unites of an energy scale  $\epsilon_0$ . We set  $\epsilon_0 = [1]$  for a convenient unit system, that also renders the time unit  $\hbar/\epsilon_0 = 1$ , thus compactifying the parameter space to  $\Theta \in [-\frac{\pi}{2}, \frac{\pi}{2}]$ . Furthermore, this parametrization of  $J$  and  $g$  makes the spectrum linearly in the particle number  $N$  in leading order.

#### A. Classical mean-field limit

We follow the standard approach [49] to derive the classical limit for bosons and replace the operators by complex numbers

$$\hat{a}_j, \hat{a}_j^\dagger \mapsto \psi_j, \psi_j^*$$

inside the normal-ordered quantum Hamiltonian Eq. (6) to get a classical mean-field system. Hamilton's equations of motion  $i\dot{\psi}_j = \frac{\partial H}{\partial \psi_j^*}$  define the classical dynamics. Due to the conserved total particle number  $N$ , we define new set of conjugated classical variables

$$\begin{aligned} N &= n_1 + n_2, & \phi &= \frac{1}{2}(\varphi_1 + \varphi_2), \\ n &= \frac{1}{2}(n_1 - n_2), & \varphi &= \varphi_1 - \varphi_2 - \pi, \end{aligned}$$

where the two mean fields  $\psi_j = \sqrt{n_j} e^{i\varphi_j}$  are written in phase  $\varphi_j$  and occupations  $n_j$ . Hence, the Hamiltonian takes the form

$$\begin{aligned} H(N, \phi, n, \varphi) &= \\ &= 2 \cos \Theta \sqrt{N^2 - 4n^2} \cos \varphi + \sin \Theta \left( \frac{2n^2}{N} + \frac{N}{2} \right). \end{aligned} \quad (7)$$

We can reduce the dynamics to an 1d-system with a single conjugated pair ( $z = \frac{2n}{N}, \varphi = \varphi_1 - \varphi_2 - \pi$ ) given by the population inversion and relative phase [50]. With

these coordinates, we can reduce the equations of motion to two coupled real-valued ODEs

$$\begin{aligned} \dot{z} &= -4 \cos \Theta \sqrt{1 - z^2} \sin \varphi, \\ \dot{\varphi} &= 4 \cos \Theta \frac{z \cos \varphi}{\sqrt{1 - z^2}} - 2 \sin \Theta z, \end{aligned} \quad (8)$$

which is an 1-degree of freedom system. Conveniently, the mean-field system Eq. (8) is exactly solvable and independent of the particle number  $N$ .

#### B. Fixed points

A straightforward calculation shows that there are two fixed points ( $z = 1, \varphi = \pi$ ) and ( $z = 1, \varphi = 0$ ) which are independent from the system parameter  $\Theta$ . We call these two FPs the hom. and antihom. FP, since both have homogeneous occupations and a zero or  $\pi$  phase difference between site one and two. We set the zero point for the relative phase  $\varphi$  to the unstable antihom FP.

Two bifurcations appear: at  $\Theta = -\arctan 2$  for the hom. FP and at  $\Theta = \arctan 2$  for antihom. FP. We restrict ourselves only to the antihom. FP, since there is a symmetry between them under change of the sign of the parameter  $\Theta$ .

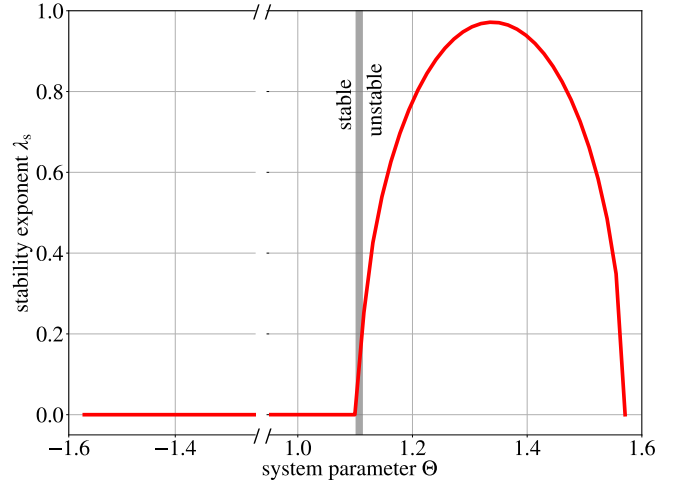


FIG. 2. Stability exponent of the antihom. FP over the whole parameter space: change from unstable to stable at the bifurcation point  $\Theta = \arctan 2$ .

The stability diagram of the antihom. FP in Fig. 2 shows the bifurcation at  $\arctan 2$ , where the stability exponent becomes positive. Its maximum  $\lambda_s = 0.97$  is reached at  $\Theta_* \approx 1.35$ .

At the maximal unstable parameter  $\Theta_*$ , Fig. 3 shows the reduced phase space structure of the system Eq. (8). Note in particular the (red) separatrix defined by the unstable and stable manifold originating from the antihom. FP. The merging of stable and unstable manifolds indicates that the linearized regime is bounded, namely, any

classical trajectory on the unstable manifolds converges to the stable manifold and (in infinite time) to the hyperbolic FP. The exact size of the linearized regime (modeled by the constant  $c$  in the previous Sec. II) plays a neglectable role for  $\hbar_{\text{eff}} \rightarrow 0$ , since it is additive and  $\hbar_{\text{eff}}$ -independent constant in the Ehrenfest time  $\tau_E$ . Therefore we leave  $c$  undefined in the subsequent discussion.

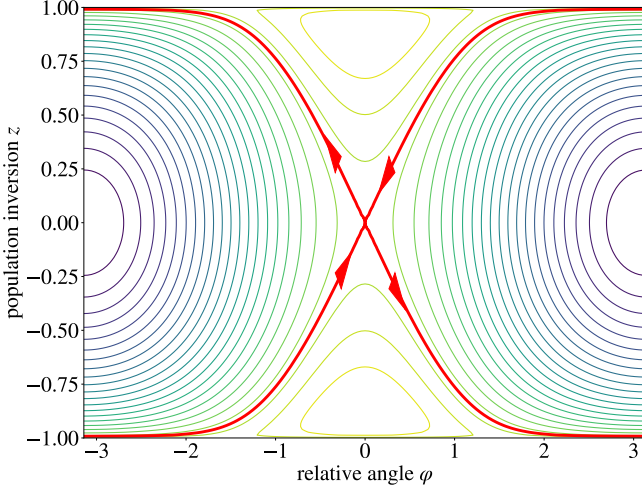


FIG. 3. Reduced phase space structure ( $z, \varphi$ ) for  $\Theta_*$ : contour lines of the Hamiltonian correspond to the classical trajectories, there are three stable fixed and one hyperbolic fixed point with its red dashed separatrix. Arrows on the separatrix indicate the stable and unstable manifolds.

We verified that, as shown in Fig. 3 for  $\Theta_*$ , we verify that this is the only unstable FP in the classical mean-field limit. This is also true for the whole range  $\Theta \in (\arctan 2, \pi/2)$ , where the antihom. FP is unstable.

Armed with this very specific phase-space structure, we carry an in-depth analytical study of the OTOC  $\mathbf{C}(t)$  for the dimer in the next section.

### C. Microscopic approach: separatrix dynamics

We set for the dimer the operators  $\hat{A} = \hat{B} = \hat{n}_1$  to be the number operator  $\hat{n}_1 = \hat{a}_1^\dagger \hat{a}_1$  at the first site. Therefore, we get

$$\mathbf{C}(t) = \langle \|\hat{n}_1(t), \hat{n}_1\| \rangle^2 = \langle \|\hat{n}(t), \hat{n}\| \rangle^2, \quad (9)$$

where  $\hat{n} = \frac{1}{2}(\hat{n}_1 - \hat{n}_2)$ . For this OTOC, we are interested in evaluating the classical expression which is given by

$$O(t) = \iint dnd\varphi W(n, \varphi) \left( \frac{\partial n_t}{\partial \varphi_0} \right)^2, \quad (10)$$

with  $W(n, \varphi)$  the Wigner function associated with the initial state. The latter is, for the sake of simplicity, modeled as a coherent quantum state  $e^{\sqrt{N_0}(\hat{a}_-^\dagger - \hat{a}_-)} |0\rangle$  with  $\hat{a}_- = \hat{a}_1 - \hat{a}_2$ , keeping in mind that for large  $N_0$

this coherent state features very similar properties as a number-projected coherent state with total particle number  $N_0$  as far as the site population exchange dynamics is concerned. The Wigner function associated with this initial state would be given by

$$W(N, \phi, n, \varphi) \simeq \frac{1}{\pi^2} \exp \left( -\frac{(N - N_0)^2}{2N_0} - 2N_0\phi^2 - \frac{2n^2}{N_0} - \frac{N_0\varphi^2}{2} \right) \quad (11)$$

in the framework of a quadratic expansion valid for  $N_0 \gg 1$  (using again  $\hbar = 1$ ). Since the Wigner function  $W$  describes a tight localization of  $N$  about  $N_0$ , we set  $N_0 = N$  henceforth and model the initial quantum state concerning the inter-site population exchange dynamics by the Wigner function

$$W(n, \varphi) = \frac{1}{\pi} \exp \left( -\frac{2n^2}{\omega N} - \frac{N\omega\varphi^2}{2} \right), \quad (12)$$

where the squeezing parameter  $\omega$  allows for some flexibility in the definition of the initial quantum state.

Let us first discuss the linearized dynamics in the near vicinity of the FP  $(n, \varphi) = (0, 0)$ . Linearizing Eq. (8), we obtain the system of equations

$$\begin{aligned} \dot{z} &= -4 \cos \Theta \varphi, \\ \dot{\varphi} &= -2(\sin \Theta - 2 \cos \Theta)z, \end{aligned} \quad (13)$$

which is readily solved as

$$\begin{aligned} z_t &= z_0 \cosh \lambda_s t - \frac{4 \cos \Theta \varphi_0}{\lambda_s} \sinh \lambda_s t, \\ \varphi_t &= \varphi_0 \cosh \lambda_s t - \frac{\lambda_s z_0}{4 \cos \Theta} \sinh \lambda_s t \end{aligned} \quad (14)$$

in terms of the stability exponent

$$\lambda_s = 4 \cos \Theta \sqrt{\frac{\gamma}{2} - 1}, \quad (15)$$

where we defined the so called nonlinearity parameter  $\gamma = \tan \Theta = \frac{gN}{LJ}$ . The latter becomes purely imaginary for  $\gamma < 2$ , which implies that  $(n, \varphi) = (0, 0)$  turns into a stable fixed point if the nonlinearity parameter  $\gamma$  is decreased below two, as it is plotted in Fig. 2.

Considering  $\gamma > 2$  henceforth, and assuming that the point  $(z_0, \varphi_0)$  is located very closely to the origin in this phase space, we can, as in the previous section, identify a time scale  $\tau_s \gg \lambda_s^{-1}$  for which we still have  $|z_{\tau_s}| \ll 1$  and  $|\varphi_{\tau_s}| \ll 1$ , such that the above linearization Eq. (13) of the classical equations of motion remains valid until  $t = \tau_s$ . Since at the same time we have  $\lambda_s \tau_s \gg 1$  by assumption, the solution Eq. (14) of the linearized Eq. (13) for  $t = \tau_s$  simplifies as

$$z_{\tau_s} = \left( \frac{z_0}{2} - \frac{2 \cos \Theta \varphi_0}{\lambda_s} \right) e^{\lambda_s \tau_s}, \quad (16)$$

$$\varphi_{\tau_s} = \left( \frac{\varphi_0}{2} - \frac{\lambda_s z_0}{8 \cos \Theta} \right) e^{\lambda_s \tau_s}. \quad (17)$$

From the time  $\tau_s$  on, we can safely assume that the trajectory under consideration very closely follows the separatrix structure emanating from the unstable antihom. fixed point  $(z, \varphi) = (0, 0)$ . This separatrix structure is obtained through the identification of the energy

$$H(n, \varphi) = 2 \cos \Theta N + \sin \Theta \frac{N}{2} \quad (18)$$

of the classical Hamiltonian Eq. (7), from which follows the identity

$$\cos \varphi = \frac{1 - \frac{\gamma}{4} z^2}{\sqrt{1 - z^2}}.$$

Inserting this expression into Eq. (8) yields the differential equation

$$\dot{z} = z \sqrt{\lambda_s^2 - \sin^2 \Theta z^2}$$

describing the motion along the upper or lower separatrix branch. This equation is straightforwardly integrated yielding

$$\begin{aligned} t - \tau_s &= \int_{z_{\tau_s}}^{z_t} \frac{dz}{z \sqrt{\lambda_s^2 - \sin^2 \Theta z^2}} \\ &= -\frac{1}{\lambda_s} \left[ \operatorname{arcosh} \left( \frac{\lambda_s}{\sin \Theta |z_t|} \right) - \operatorname{arcosh} \left( \frac{\lambda_s}{\sin \Theta |z_{\tau_s}|} \right) \right], \end{aligned}$$

from which we obtain

$$z_t = \frac{\operatorname{sgn}(z_{\tau_s}) \lambda_s / \sin \Theta}{\cosh \left[ \operatorname{arcosh} \left( \frac{\lambda_s}{\sin \Theta |z_{\tau_s}|} \right) - \lambda_s (t - \tau_s) \right]}. \quad (19)$$

Using  $|z_{\tau_s}| \ll 1$  and hence also  $\sin \Theta |z_{\tau_s}| / \lambda_s \ll 1$  for finite values of  $\sin \Theta$  and  $\lambda_s$ , we define

$$\begin{aligned} x_t &= \operatorname{sgn}(z_{\tau_s}) \exp \left[ -\operatorname{arcosh} \left( \frac{\lambda_s}{\gamma |z_{\tau_s}|} \right) + \lambda_s (t - \tau_s) \right] \\ &\simeq \frac{\sin \Theta}{2 \lambda_s} \left( \frac{z_0}{2} - 2 \cos \Theta \frac{\varphi_0}{\lambda_s} \right) e^{\lambda_s t} \\ &\simeq \frac{\sin \Theta}{\lambda_s} \left( \frac{n_0}{N} - 2 \cos \Theta \frac{\varphi_0}{\lambda_s} \right) \sinh(\lambda_s t), \end{aligned} \quad (20)$$

where we make use of the asymptotic expression

$$\operatorname{arcosh}(u) = \ln \left( u + \sqrt{u^2 - 1} \right) \simeq \ln(2u) + O(u^{-2}) \quad (21)$$

for large  $u$ , in combination with Eq. (16). With  $(\cosh u)^{-1} = 2e^u/(1 + e^{2u})$  together with Eqs. (21) and (20), Eq. (19) yields

$$z_{\tau} = \frac{2 \lambda_s}{\sin \Theta} \frac{x_t}{1 + x_t^2} \quad (22)$$

and thus

$$n_t = \frac{N \lambda_s}{\sin \Theta} \frac{x_t}{1 + x_t^2}. \quad (23)$$

Replacing  $e^{\lambda_s t}$  with  $2 \sinh(\lambda_s t)$  in Eq. (20) is clearly valid for large  $\lambda_s t \gg 1$  and has the additional advantage that the short-time regime in the time evolution of  $n_t$  will thereby be correctly captured as well within Eq. (23).

The classical limit of the quantum OTOC, Eq. (10), is then evaluated as

$$\begin{aligned} O(t) &= \frac{2 \cos^2 \Theta N^2}{\sqrt{\pi} a \lambda_s^2} \sinh(\lambda_s t) \\ &\quad \int \frac{(1 - x^2)^2}{(1 + x^2)^4} \exp \left[ -\left( \frac{x}{2a \sinh(\lambda_s t)} \right)^2 \right] dx \end{aligned} \quad (24)$$

where the dimensionless scale is defined as

$$a = \frac{\sin \Theta / \lambda_s}{\sqrt{8 \omega N}} \sqrt{\omega^2 + \frac{16 \cos^2 \Theta}{\lambda_s^2}}. \quad (25)$$

The short-time behavior of the OTOC, for  $t \ll \tau_L = -\lambda_s^{-1} \ln a$ , is yielded as

$$O(t) \simeq 4 \cos^2 \Theta \frac{N^2}{\lambda_s^2} \sinh^2(\lambda_s t), \quad (26)$$

while for  $t \gg \tau_L$  we obtain

$$O(t) \simeq \cos^2 \Theta \frac{\sqrt{\pi} N^2}{4a \lambda_s^2} e^{\lambda_s t}. \quad (27)$$

These two limits correspond to the heuristic derived  $2\lambda_s - \lambda_s$  transition Eq. (5) in the previous Sec. II. Note the here defined  $\tau_L$  agrees with the case ii) in Sec. II. The dimensionless constant  $\ln a$  encodes the linear width of the wave-packet along the unstable direction.

With this extensive classical calculation at hand, we analyze the OTOC centered around this local hyperbolic antihom. FP using  $\Theta_*$  at the maximal value of the stability exponent  $\lambda_s = 0.97$ .

#### D. Numerical results for the Out-of-Time-Order Correlator

We proceed now with the numerical study and calculate the OTOC via Eq. (9) by means of extensive numerically exact simulations for the operators  $\hat{A} = \hat{B} = \hat{n}_1$ . We will consider the state

$$|\vec{\xi}\rangle = \frac{1}{\mathcal{N}} (\vec{\xi} \cdot \hat{a}^\dagger)^N |0\rangle,$$

which is a number-projected coherent state centered at the antihom. FP  $\vec{\xi} = (\sqrt{N/2}, -\sqrt{N/2})$ , with  $\mathcal{N} = \sqrt{N^N N!}$  a normalization constant.

For large total particle number  $N$ , the projected coherent state inherits properties from the coherent state, in particular the linear width of  $\hbar_{\text{eff}}^{1/2}$  in each phase space direction [51], including the unstable direction in Fig. 3. Furthermore it sets the squeezing parameter  $\omega = 1$  in the classical analysis in Eq. (25). Following the discussion in

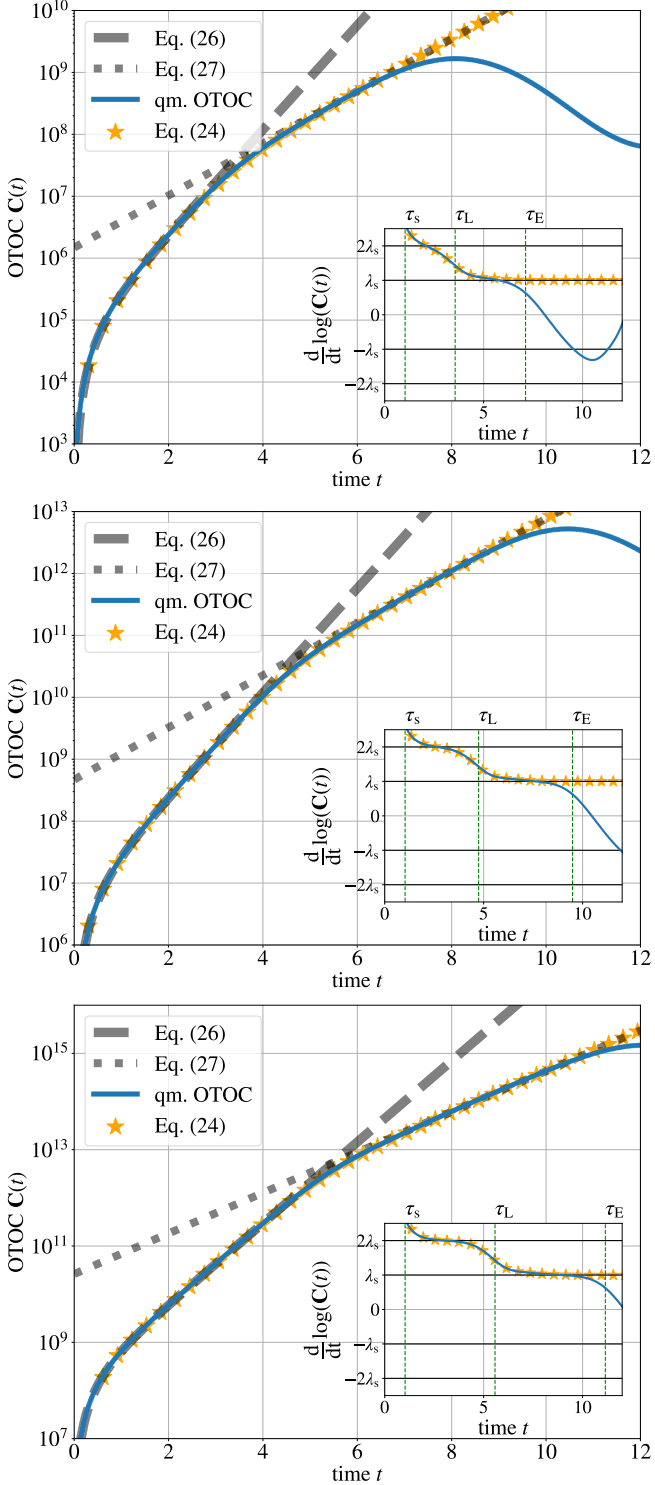


FIG. 4. Top to bottom: OTOC  $\mathbf{C}(t)$  for  $N = 10^3, 10^4, 5 \cdot 10^4$  and  $\Theta = 1.35$ ; shaping kink from the  $2\lambda_s - \lambda_s$  transition at  $\tau_L = \tau_E/2$ ; the classical expressions Eq. (26) and Eq. (27) fit tightly the OTOC in each region showing  $e^{2\lambda_s t}$  and  $e^{\lambda_s t}$  exponential growth rates.

Sec. II, case ii), the leaking time  $\tau_L$  is therefore half the Ehrenfest time  $\tau_E$ . We display our numerical OTOCs for

increasing particle  $N = 10^3, 10^4, 5 \cdot 10^4$  in Fig. 4, where we observe the predicted  $2\lambda_s - \lambda_s$  transition, precisely following the heuristic arguments of Sec. II and the exact analysis of Sec. III C. In particular, the analytical result for the classical OTOC Eq. (24) follows perfectly the quantum OTOC  $\mathbf{C}(t)$ , i.e., it captures both regimes and the transition. The kink at the transition gets sharper for  $N \rightarrow \infty$ . Here, the insets showing the time-derivative of  $\log(\mathbf{C}(t))$  confirm a more and more pronounced  $2\lambda_s$  and  $\lambda_s$  regions of exponential growth.

In order to justify the leaking from the linearized region around the FP, we visualize the time dynamical evolution of the Husimi distribution for  $N = 10^3$  in Fig. 5. With time, the linear width of the wave-packet increases and evolves to the upper right and lower left corner of the phase space. We recognize that at time  $\tau_L = \tau_E/2$  the wave-packet folds back from the unstable to the stable manifold. This back-folding corresponds to the dynamical transition of leaking from the linearized regime.

The excellent agreement between our physical picture based on the leaking mechanism and the numerical simulations opens the possibility of manipulating the leaking time  $\tau_L$ , and therefore the different scrambling regimes, via squeezing the initial state  $|\vec{\xi}\rangle$ , as we discuss next.

### E. Squeezing – engineering the leaking time $\tau_L$

An important consequence of the leaking mechanism is that the linear width of the initial state along the unstable manifolds is the key ingredient for the exact position of the  $2\lambda_s - \lambda_s$  transition.

In order to check this dependence, we proceed to squeeze the coherent state on the antihom. FP and subsequently calculate the OTOC. Interestingly, squeezed states in optical lattices can be archived experimentally [39] to an excellent degree. In our theoretical setup, squeezing protocol can be effectively (and unitarily) realized by the reversing the time evolution itself. This means, we replace  $|\xi\rangle$  by

$$|\xi(t_0)\rangle = \hat{U}(t_0)|\xi\rangle$$

with  $t_0 = -\tau_E/2$ , where  $\hat{U}(t_0)$  is the time-evolution operator, and then calculate the OTOC Eq. (1) for the initial state  $\hat{\rho}(t_0) = |\xi(t_0)\rangle\langle\xi(t_0)|$ . The corresponding scrambling dynamics is shown in then the left panel of Fig. 6 for  $N = 10^3$ , while the right panel depicts the initial Husimi distribution of the squeezed state. This backward-time evaluated coherent state has a reduced linear width along the unstable manifold by taking  $t_0$  to  $-\tau_E/2$  (for the non-squeezed coherent state), i.e., we transform  $\Delta u \sim \hbar_{\text{eff}}^{1/2}$  to  $\Delta u \sim \hbar_{\text{eff}}$ . Thus, the new leaking time  $\tau_L^*$  is at the Ehrenfest time and no  $2\lambda_s - \lambda_s$  transition is expected to exist, as fully confirmed by the numerical simulations.

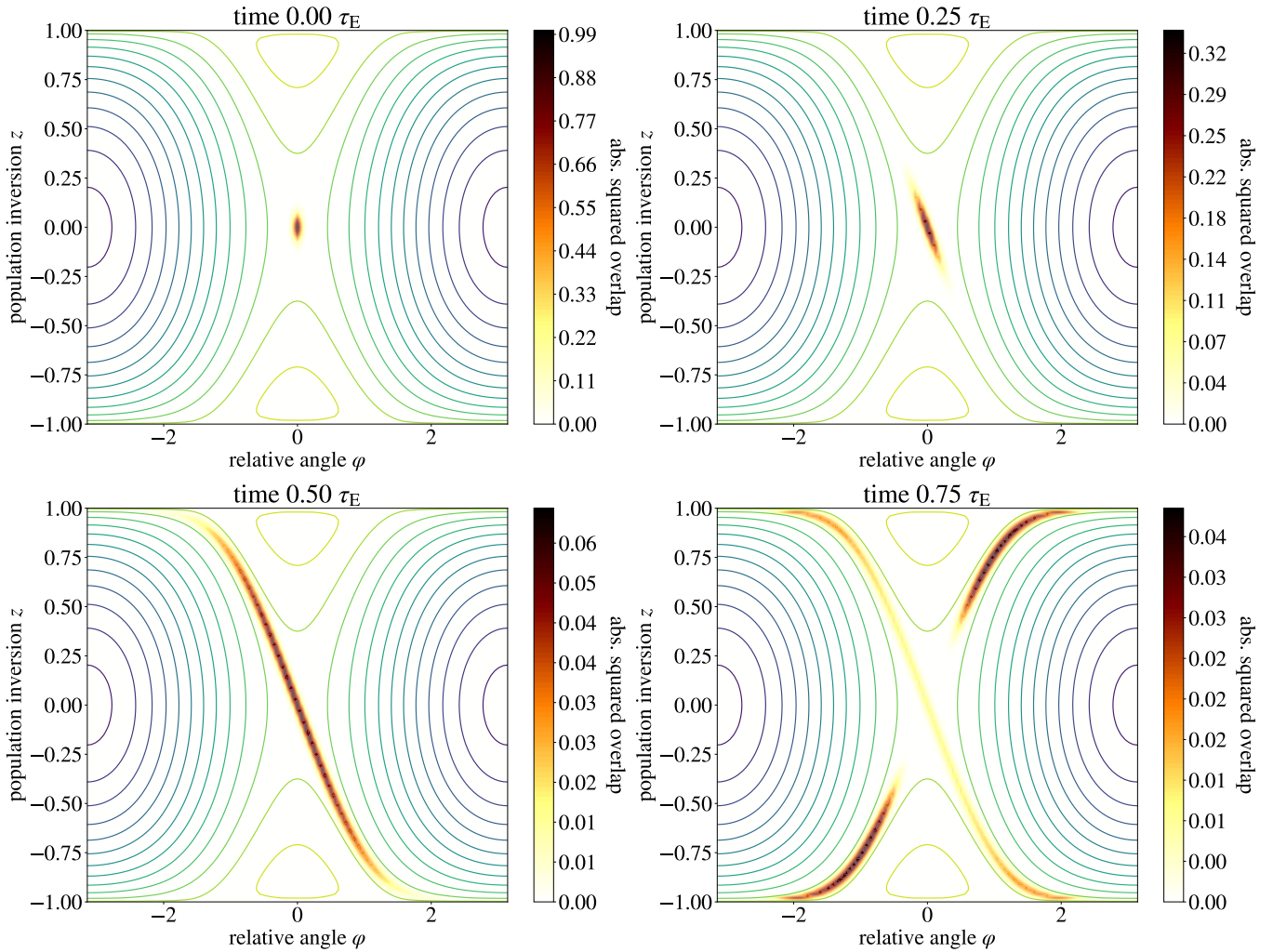


FIG. 5. Time-evolution of the Husimi-distribution for the state  $|\vec{\xi}\rangle$  centered at the hyperbolic antihom. FP with  $N = 10^3$  particles, we observe scrambling along the unstable manifold on the separatrix until  $t \approx \tau_L$ .

#### F. OTOC – parameter scan

So far, we handpicked one of the most unstable configuration for the antihom. FP and did not perform a fitting with an exponential function beyond the visual agreement in Figs. 4 and 6. We now show the results of a proper fitting procedure in Fig. 7 for the number projected state  $|\vec{\xi}\rangle$ . Here, we show the fitted quantum Lyapunov exponents  $\lambda_q$  of the OTOC in both regions  $[\tau_s, \tau_L]$  and  $[\tau_L, \tau_E]$  along the whole parameter range of  $\Theta$  and for several values of the total particle number  $N$ . We see an increasing agreement with the  $2\lambda_s$ - and  $\lambda_s$ -regions: the fitted exponents show the same  $\Theta$ -dependency as the stability exponent  $\lambda_s$ . Further, their magnitudes approach the classical value with  $\hbar_{\text{eff}} \rightarrow 0$ . The discrepancy originates from the fitting procedure, as it ignores the transition between the two exponential regimes. We conclude that the  $2\lambda_s - \lambda_s$  transition is independent of the specific value of  $\Theta$ , i.e., it is a robust signal of a dynamical

transition.

## IV. CONCLUSION & OUTLOOK

#### A. Conclusion – integrable systems

A localized wavepacket around a hyperbolic fixed point in a quantum system with integrable classical (mean-field) limit undergoes a transition between different dynamical regimes driven by a leaking mechanism of phase space volume along classical separatrices. If located within the pre-Ehrenfest time scale, this dynamical transition imprints a characteristic kink structure to the scrambling as measured by the exponential form of out-of-time-order correlators. Specifically, the exponential growth changes from  $2\lambda_s$  to  $\lambda_s$  and the kink develops for  $\hbar_{\text{eff}} \rightarrow 0$  where  $\lambda_s$  is the stability exponent of the fixed point. We have derived an analytical theory and shown how this behavior is actually directly related to the clas-

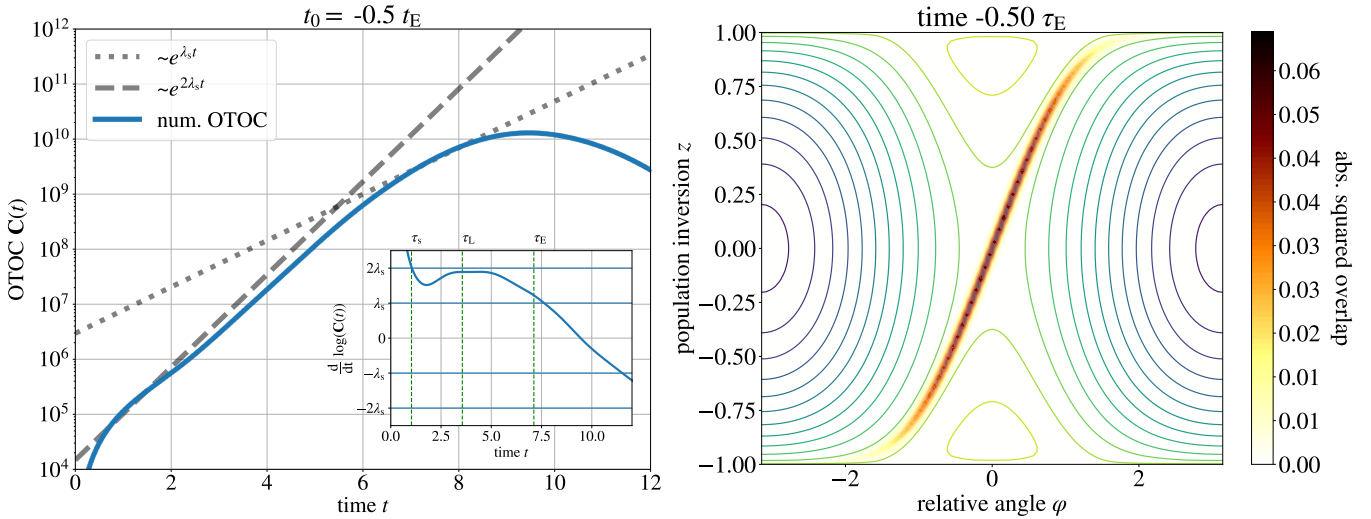


FIG. 6. Left panel: OTOC for a squeezed coherent state for the system parameter  $\Theta = 1.35$  and particle number  $N = 10^3$ ; the transition to  $\lambda_s$  vanishes. Right panel: Husimi distribution of the squeezed coherent state. The state is distributed along the stable and localized  $\sim \hbar_{\text{eff}}$  along the unstable manifold.

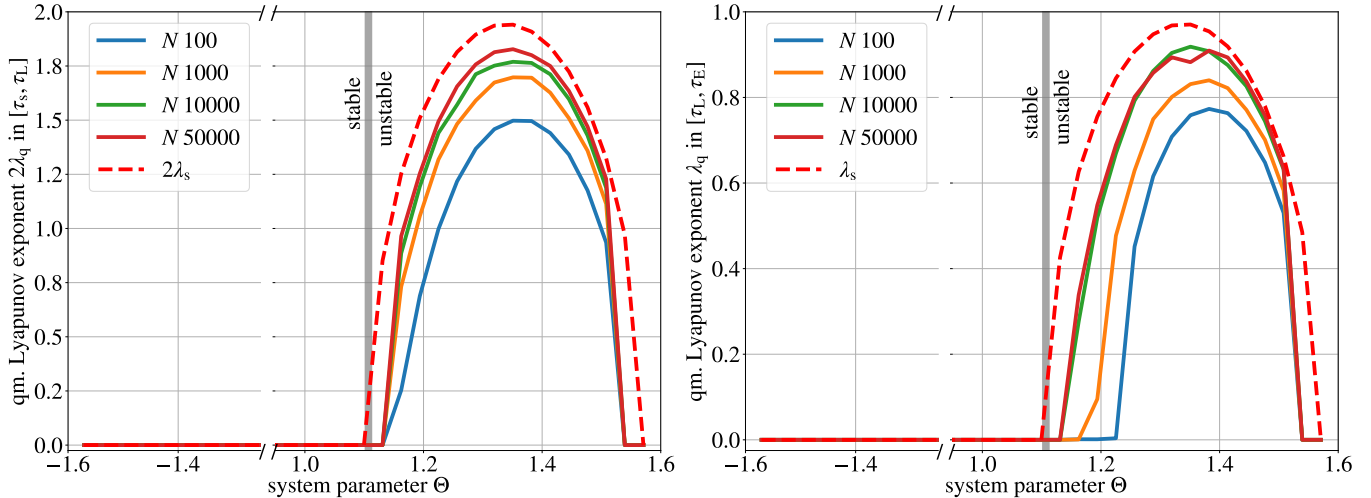


FIG. 7. Fitted exponents for the  $2\lambda_s$  (upper panel) and the  $\lambda_s$  (lower panel) region; for  $N \rightarrow \infty$ , we see an increasing agreement with the classical predictions from Eq. (5).

sical limit of the out-of-time-order correlators when their time dependence is governed by the separatrix dynamics emerging around an unstable FP.

Following this picture, we have shown that squeezing the initial coherent state allows us to engineer the leaking time and thus the dynamical transition itself exactly as predicted by our analytical considerations.

If the phase-space localization scale of the initial state is strong enough, the leaking time is beyond the Ehrenfest time and we obtain the standard  $2\lambda_s$  exponent. In contrast, an uniform state starts to leak immediately and even before the ergodic time. Therefore, the infinite temperature OTOC grows only with the reduced exponent  $\lambda_s$ .

We have supported our picture of the dynamical transi-

tion by means of extensive simulations on the experimentally accessible, and integrable, Bose-Hubbard dimer. The extremely clean fixed-point and separatrix structure of this systems allows us for a detailed study of the mechanism and the analytical expectations of Sec. II are verified to an excellent degree.

## B. Outlook – beyond integrability

In order to focus on the separatrix effects like the leaking mechanism, a very well controlled classical phase space is required, so our numerical findings and the corresponding analytical theory has been restricted so far to an integrable system where the theory in Sec. II

assumes a bounded linearized regime around the fixed point. In order to transfer this concepts to the realm of chaotic systems, a straightforward generalization is to assume a bounded Lyapunov zone inside a chaotic region, i.e., a finite deviation  $\delta x_0$  grows only for a finite time like  $\delta x(t) \sim e^{\lambda_L t} \delta x_0$ . Following this idea, the role of the stability exponent  $\lambda_s$  from the fixed point is now translated to the Lyapunov exponent  $\lambda_L$  of the chaotic sea. An open question is if a wave-packet is actually sensitive to leaking out of the Lyapunov zone. Unlike the presented integrable case, the source of instability is the non-local whole mixing chaotic sea conflicting the idea of a leaking wave-packet, a question that is now under investigation.

Lacking of a full-fledged analytical approach for chaotic systems, one option is to turn to an effective type of description. A first numerical exploration of this matter can be found in [52], where the authors treat the combination of unstable fixed points and chaotic layers investigating

the role of the stability exponent  $\lambda_s$  versus the Lyapunov exponent  $\lambda_L$  for pre-Ehrenfest time scales.

In such a situation, it is an open and thrilling question whether the  $2\lambda_s - \lambda_s$  transition could distinguish a chaotic from an integrable system. In the same vein, we may ask the immediate question, whether this transition can be generalized in the mixed dynamics, as a series of different exponential growth regions given by several different local Ehrenfest times.

## V. ACKNOWLEDGMENTS

We are grateful for financial support from the Deutsche Forschungsgemeinschaft (German Research Foundation) through Project Ri681/15-1 within the Reinhart-Koselleck Programme. MS further acknowledges funding through the Studienstiftung des Deutschen Volkes.

---

[1] Q. Hummel, B. Geiger, J. D. Urbina, and K. Richter, Phys. Rev. Lett. **123**, 160401 (2019).

[2] T. Xu, T. Scaffidi, and X. Cao, Phys. Rev. Lett. **124**, 140602 (2020).

[3] S. Xu and B. Swingle, (2022), arXiv:2202.07060 [quant-ph].

[4] K. Richter, J. D. Urbina, and S. Tomsovic, Journal of Physics A: Mathematical and Theoretical **55**, 453001 (2022).

[5] J. Maldacena, S. H. Shenker, and D. Stanford, Journal of High Energy Physics **2016** (2016).

[6] P. Hayden and J. Preskill, Journal of High Energy Physics **2007**, 120 (2007).

[7] Y. Sekino and L. Susskind, arXiv:0808.2096 [hep-th].

[8] Y. Gu and A. Kitaev, Journal of High Energy Physics **2019** (2019), 10.1007/jhep02(2019)075.

[9] B. Kobrin, Z. Yang, G. D. Kahanamoku-Meyer, C. T. Olund, J. E. Moore, D. Stanford, and N. Y. Yao, Phys. Rev. Lett. **126**, 030602 (2021).

[10] N. Tsuji and P. Werner, Phys. Rev. B **99**, 115132 (2019).

[11] A. I. Larkin and Y. N. Ovchinnikov, Soviet Journal of Experimental and Theoretical Physics **28**, 1200 (1969).

[12] B. Swingle, G. Bentsen, M. Schleier-Smith, and P. Hayden, Phys. Rev. A **94**, 040302 (2016).

[13] M. Gärttner, J. G. Bohnet, A. Safavi-Naini, M. L. Wall, J. J. Bollinger, and A. M. Rey, Nature Physics **13**, 781 (2017).

[14] J. Li, R. Fan, H. Wang, B. Ye, B. Zeng, H. Zhai, X. Peng, and J. Du, Phys. Rev. X **7**, 031011 (2017).

[15] R. A. Kidd, A. Safavi-Naini, and J. F. Corney, Phys. Rev. A **102**, 023330 (2020).

[16] H. Shen, P. Zhang, R. Fan, and H. Zhai, Phys. Rev. B **96**, 054503 (2017).

[17] A. Bohrdt, C. B. Mendl, M. Endres, and M. Knap, New Journal of Physics **19**, 063001 (2017).

[18] S. Pappalardi, A. Russomanno, B. Žunkovič, F. Iemini, A. Silva, and R. Fazio, Phys. Rev. B **98**, 134303 (2018).

[19] D. Villaseñor, S. Pilatowsky-Cameo, M. A. Bastarrachea-Magnani, S. Lerma-Hernández, L. F. Santos, and J. G. Hirsch, Entropy **25** (2023), 10.3390/e25010008.

[20] L. Benet, F. Borgonovi, F. M. Izrailev, and L. F. Santos, (2022), arXiv:2211.10451 [cond-mat.stat-mech].

[21] S. Pilatowsky-Cameo, J. Chávez-Carlos, M. A. Bastarrachea-Magnani, P. Stránský, S. Lerma-Hernández, L. F. Santos, and J. G. Hirsch, Phys. Rev. E **101**, 010202 (2020).

[22] R. A. Kidd, A. Safavi-Naini, and J. F. Corney, Phys. Rev. A **103**, 033304 (2021).

[23] K. Hashimoto, K.-B. Huh, K.-Y. Kim, and R. Watanabe, Journal of High Energy Physics **2020** (2020), 10.1007/jhep11(2020)068.

[24] J. Rammensee, J. U. Urbina, and K. Richter, Phys. Rev. Lett. **121**, 124101 (2018).

[25] I. García-Mata, M. Saraceno, R. A. Jalabert, A. J. Roncaglia, and D. A. Wisniacki, Phys. Rev. Lett. **121**, 210601 (2018).

[26] E. Fortes, I. García-Mata, R. Jalabert, and D. Wisniacki, Physical Review E **100** (2019), 10.1103/PhysRevE.100.042201.

[27] A. Polkovnikov, K. Sengupta, A. Silva, and M. Vengalattore, Rev. Mod. Phys. **83**, 863 (2011).

[28] W. P. Schleich, *Quantum Optics in Phase Space* (Wiley-VCH, Berlin, 2001).

[29] Y. S. Kim and M. E. Noz, *Phase Space Picture of Quantum Mechanics* (World Scientific, 1991).

[30] R. F. O'Connell, International Journal of Quantum Information **06**, 415 (2008).

[31] M. Gutzwiller, *Chaos in Classical and Quantum Mechanics*, Interdisciplinary Applied Mathematics (Springer New York, 1991).

[32] F. Haake, *Quantum Signatures of Chaos*, Physics and astronomy online library (Springer, 2001).

[33] M. Brack and R. Bhaduri, *Semiclassical Physics*, Frontiers in physics (Avalon Publishing, 1997).

- [34] M. Akila, D. Waltner, B. Gutkin, P. Braun, and T. Guhr, Phys. Rev. Lett. **118**, 164101 (2017).
- [35] P. Braun, D. Waltner, M. Akila, B. Gutkin, and T. Guhr, Phys. Rev. E **101**, 052201 (2020).
- [36] T. Engl, J. D. Urbina, and K. Richter, Phys. Rev. E **92**, 062907 (2015).
- [37] M. Tabor, *Chaos and Integrability in Nonlinear Dynamics: An Introduction* (Wiley, 1989).
- [38] S. Wiggins, *Introduction to Applied Nonlinear Dynamical Systems and Chaos*, Texts in Applied Mathematics (Springer New York, 2003).
- [39] J. Estève, C. Gross, A. Weller, S. Giovanazzi, and M. K. Oberthaler, Nature **455**, 1216 (2008).
- [40] R. A. Jalabert, I. García-Mata, and D. A. Wisniacki, Phys. Rev. E **98**, 062218 (2018).
- [41] B. Geiger, *From few to many particles: Semiclassical approaches to interacting quantum systems*, Vol. 55 (University of Regensburg, 2020).
- [42] E. Il'ichev, M. Grajcar, R. Hlubina, R. P. J. IJsselnsteijn, H. E. Hoenig, H.-G. Meyer, A. Golubov, M. H. S. Amin, A. M. Zagorskin, A. N. Omelyanchouk, and M. Y. Kupriyanov, Phys. Rev. Lett. **86**, 5369 (2001).
- [43] M. Albiez, R. Gati, J. Fölling, S. Hunsmann, M. Crisostomi, and M. K. Oberthaler, Phys. Rev. Lett. **95**, 010402 (2005).
- [44] S. Fölling, S. Trotzky, P. Cheinet, M. Feld, R. Saers, A. Widera, T. Müller, and I. Bloch, Nature **448**, 1029 (2007).
- [45] D. Witthaut, F. Trimborn, and S. Wimberger, Phys. Rev. Lett. **101**, 200402 (2008).
- [46] P. Cheinet, S. Trotzky, M. Feld, U. Schnorrberger, M. Moreno-Cardoner, S. Fölling, and I. Bloch, Phys. Rev. Lett. **101**, 090404 (2008).
- [47] E. Kierig, U. Schnorrberger, A. Schietinger, J. Tomkovic, and M. K. Oberthaler, Phys. Rev. Lett. **100**, 190405 (2008).
- [48] J. Tomkovič, W. Muessel, H. Strobel, S. Löck, P. Schlagheck, R. Ketzmerick, and M. K. Oberthaler, Phys. Rev. A **95**, 011602 (2017).
- [49] J. Negele and H. Orland, *Quantum Many Particle Systems* (Basic Books, 1995).
- [50] D. K. Campbell, *The Remarkable BEC Dimer* (Springer International Publishing, Cham, 2020) pp. 247–258.
- [51] C. Gardiner, P. Zoller, and P. Zoller, *Quantum Noise: A Handbook of Markovian and Non-Markovian Quantum Stochastic Methods with Applications to Quantum Optics*, Springer Series in Synergetics (Springer, 2004).
- [52] F. Meier, M. Steinhuber, J. D. Urbina, D. Waltner, and T. Guhr, (2023), arXiv:2211.12147 [quant-ph].